Pressure dependence of the sound velocity in a two-dimensional lattice of Hertz-Mindlin balls: Mean-field description

B. Velický* and C. Caroli
Groupe de Physique des Solides, 2 place Jussieu, 75251 Paris Cedex 05, France†
(Received 25 July 2001; published 25 January 2002)

We study the dependence on the external pressure P of the velocities $v_{L,T}$ of long wavelength sound waves in a confined two-dimensional hexagonal close-packed lattice of 3D elastic frictional balls interacting via one-sided Hertz-Mindlin contact forces, whose diameters exhibit mild dispersion. The presence of an underlying long range order enables us to build an effective medium description, which incorporates the radial fluctuations of the contact forces acting on a single site. Due to the nonlinearity of Hertz elasticity, self-consistency results in a highly nonlinear differential equation for the ''equation of state'' linking the effective stiffness of the array with the applied pressure, from which sound velocities are then obtained. The results are in excellent agreement with existing experimental results and simulations in the high- and intermediate-pressure regimes. It emerges from the analysis that the departure of $v_L(P)$ from the ideal $P^{1/6}$ Hertz behavior must be attributed primarily to the fluctuations of the stress field, rather than to the pressure dependence of the number of contacts.

DOI: 10.1103/PhysRevE.65.021307 PACS number(s): 45.70.−n, 43.40.+s

I. INTRODUCTION

Sound propagation in a dry confined granular medium still is, to a large extent, an open question. In particular, a long-standing puzzle is concerned with explaining the dependence of sound velocities on the externally applied pressure P.

The load bearing intergrain contacts, which ensure the mechanical stability of the packing, are of the Hertz type, i.e., their longitudinal stiffness (along the intercenter axis) scales as $F^{1/3}$, with F being the corresponding load. As shown by Mindlin [1], this scaling also holds, for frictional balls, for their shear stiffness, provided that the shear load borne by the contact is much smaller than the friction threshold. So, one intuitively expects that the velocity of, say, longitudinal sound $v_L \sim P^{1/6}$.

However, experimental results depart strongly from this expectation: v_L is found to exhibit a much faster P dependence, which is commonly characterized by ''effective exponents'' $\nu = d(\ln v)/d(\ln P)$. Values of ν of order roughly $\frac{1}{4}$ are often mentioned. Such a behavior is observed for three-dimensional (3D) random grain packings, which present what we will term ''strong topological disorder'' but also, more surprisingly, for artificially built regular arrays of quasimonodisperse balls. This was first shown on a 3D fcc lattice by Duffy and Mindlin [2], who found that the faster dependence with $\nu \sim \frac{1}{4}$ in the intermediate-pressure range tended asymptotically, at high P's, towards the Hertz $P^{1/6}$ dependence. Recently, Gilles and Coste [3] have investigated in detail sound propagation in a 2D hexagonal lattice of steel balls. Their experimental results for $v_L(P)$, which are qualitatively similar to those of Duffy and Mindlin, have motivated the present study.

Various explanations for this behavior for strongly disordered packings have been put forward. In particular, Goddard [4] proposed that a $\frac{1}{4}$ value of ν might originate from the existence of conical contacts, while de Gennes [5] suggested that the presence of heterogeneous shells surrounding the grain bodies might in some cases be relevant. A possibly more natural explanation lies in the pressure dependence of the number of load bearing contacts in the packing. It has been at the center of several recent works. In particular, a direct numerical study by Makse *et al.* [6] demonstrates the correlation between number of contacts and sound velocity in a 3D system.

For regular arrays, such an explanation may at first appear doubtful. However, Roux [7] has studied numerically the 2D hexagonal close-packed (hcp) structure and found that even a minute dispersion in ball radii leads to a similar effect. Namely, due to purely geometrical constraints, as the pressure increases, the average number of contacts per ball N_c varies from ~ 2.5 at the rigidity threshold to its maximum value of 6 at high P.

Although such effects seem to be within the reach of a mean-field description, the various attempts in this direction have up to now failed to account for deviations from the Hertz power law [8–10]. As already suggested by Makse *et al.* [6], we believe this to result from the central but implicit assumption of these models that the local contact arrangement deforms homothetically when P changes. This amounts to neglecting the essential effect of local stress inhomogeneities: due to the elastic Hertz deformations, they result in a dispersion of intercenter distances, and hence of the bond strengths. In other words, even in the absence of a change in contact number, the change of bond stiffness induced by a pressure change is nonaffine.

While it is certainly very difficult to improve upon this approximation in the case of strong topological disorder, the case of a periodic array of weakly disperse balls seems ame-

*Permanent address: Faculty of Mathematics and Physics, Charles University, Ke Karlovn 5, 121 16 Praha 2, Czech Republic.
†Associé au Centre National de la Recherche Scientifique et aux Universités Paris VI et VII.

nable to a realistic description. Indeed, in this case, the existence of a reference lattice permits to formulate a mean-field theory in the spirit of the single center self-consistent coherent potential approximation approach [11], developed already long ago to describe the electronic properties of metallic alloys. Such a route was already explored in a series of papers on depleted elastic networks [12,13]. However, in these works, the distribution of active contacts was assumed to be known and independent of the external stress, and the self-consistent condition was formulated in terms of a single-bond approximation, in the spirit of Kirkpatrick's approach to percolation problems [14].

In this paper, we build an effective medium description of a 2D hcp array of Hertz-Mindlin balls, which does account for local deformation due to the disorder in ball radii. In contrast with previous theories, our self-consistency condition does depend on the global external stress. Clearly, in such a system, the higher the external pressure, the smaller the relative disorder. So, our mean field appears as a high-P expansion. It therefore complements the numerical studies of Roux, which deal with the low-P regime where percolation effects are dominant.

We show that our predictions account quantitatively for the experimental results of Gilles and Coste. Moreover, comparison with Roux's results in an overlapping intermediate-pressure range allows us to determine the range of validity of our effective medium approach. We find that it holds down to pressures where N_c has decreased by about 15% of its saturation value. From all this, we conclude that the basic physical effect responsible for departures from the $P^{1/6}$ law is, rather than the variation of contact number in itself, the disorder induced spatial stress fluctuations.

The paper is organized as follows. In Sec. II we set the basis of our model by writing the dynamical equations for a set of Hertz-Mindlin contacts under equilibrium forces aligned with the intercenter directions, and solve them for an ideal lattice of perfectly identical balls. In Sec. III, we build up our mean-field description, apply it to the hcp lattice, and obtain from it the equation of state, i.e., the force-displacement relation from which the effective bulk and shear moduli are derived. Section IV compares in detail the mean-field predictions with the experimental and numerical results.

II. BASIC MODEL AND DYNAMICAL EQUATIONS

A. Equations of motion

Let us first consider two spherical balls labeled i,j of radii d_i, d_j made of the same material, of Young modulus E, Poisson ratio σ, density ρ. The balls at equilibrium are in Hertz contact [1] under a force f directed along the intercenter axis ij, i.e., normal to the contact circle.

The normal force f displaces the intercenter distance from $d_{ij}=\frac{1}{2}(d_i+d_j)$ to $a_{ij}=d_{ij}-\delta_{ij}$, and

$$\delta_{ij}(f)=\left(\frac{9f^2}{4d_{ij}^{*}E^{*2}}\right)^{1/3}. \tag{1}$$

Due to solid friction, when submitted to a tangential force smaller than the friction threshold $\mu_s f$, the contact is pinned and cannot slide. The elastic response of this system to small additional forces δf_x, δf_y in the (x,y) plane is described, in the linear approximation, by two stiffness coefficients, given by the Hertz-Mindlin expressions, namely [1], (i) compression (normal) stiffness

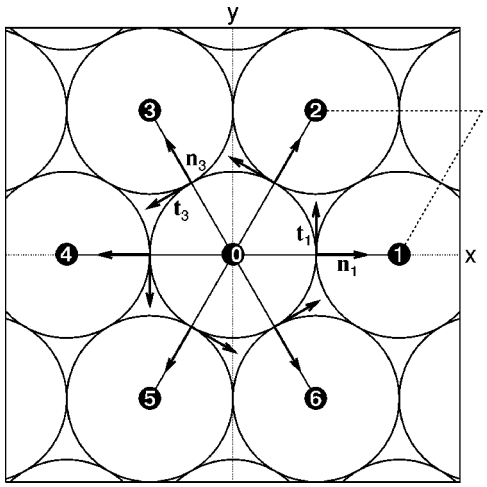

FIG. 1. Sketch of the ideal 2D hcp lattice.

$$k_{ij}=-\frac{\delta f_x}{\delta x_{ij}}=(\tfrac{3}{2}E^{*2}d_{ij}^{*}f)^{1/3} \tag{2}$$

where

$$E^{*}=\frac{E}{2(1-\sigma^2)}, \quad (d_{ij}^{*})^{-1}=\tfrac{1}{2}(d_i^{-1}+d_j^{-1}); \tag{3}$$

(ii) shear (tangential) stiffness

$$\kappa_{ij}=\eta k_{ij}, \quad \eta=\frac{2(1-\sigma)}{2-\sigma}. \tag{4}$$

Let us insist here that the fact that the ratio $\eta=\kappa_{ij}/k_{ij}$ is a mere material parameter, independent of the values of the equilibrium forces, only holds for the case of a purely normal equilibrium loading, which we assume to be the case here. In the general situation with a finite equilibrium tangential load f_t, $\eta\to\eta[1-(f_t/\mu_s f)^{1/3}]$. In the following, we will restrict ourselves to situations where all (equilibrium and nonequilibrium) interball forces are near normal, so that both the static and dynamic shear responses are described by the linear shear stiffness [Eq. (4)].

Small displacements of the balls can be decomposed into rigid translations $\mathbf{u}_i$, $\mathbf{u}_j$ and rotations about Oz by angles ϕ_i, ϕ_j. Denoting by $\hat{\mathbf{n}}_{ij}$, $\hat{\mathbf{t}}_{ij}$ the unit vectors normal and tangents to the (ij) contact with $\hat{\mathbf{n}}_{ij}$ directed from i to j (see Fig. 1), one immediately finds that the force and torque on ball i associated with the ij contact read, respectively,

$$\delta\mathbf{F}_{i,j}=k_{ij}[(\mathbf{u}_i-\mathbf{u}_j)\cdot\hat{n}_{ij}]\hat{\mathbf{n}}_{ij}+\eta k_{ij}[(\mathbf{u}_i-\mathbf{u}_j)\cdot\hat{\mathbf{t}}_{ij}]\hat{\mathbf{t}}_{ij} - \eta k_{ij}\tfrac{1}{2}(d_j\phi_j+d_i\phi_i)\hat{\mathbf{t}}_{ij}, \tag{5}$$

$$\delta C_{i,j} = \eta k_{ij} \frac{d_i}{2} [(\mathbf{u}_{ij} - \mathbf{u}_i) \cdot \hat{\mathbf{t}}_{ij} - \tfrac{1}{2}(d_j \phi_j + d_i \phi_i)], \quad (6)$$

and, in the small displacement limit appropriate to sound propagation, the equations of motion for a 2D lattice of balls are

$$M_i \ddot{\mathbf{u}}_i = \sum_{\{j\}} \delta \mathbf{F}_{i,j}, \quad M_i = \frac{\pi \rho d_i^3}{6}, \quad (7)$$

$$I_i \ddot{\phi}_i = \sum_{\{j\}} \delta C_{i,j}, \quad I_i = \frac{d_i^2 M_i}{10}, \quad (8)$$

where the sums are restricted to nearest neighbors in direct contact with i.

B. Ideal hcp lattice

We now consider the ideal case of a 2D hcp lattice of balls of equal diameter d prepared so that, at equilibrium, the interball forces, of magnitude f, are directed along the normals to the contacts $\hat{n}_i$ (see Fig. 1). Such a "hydrostatic" configuration can be realized by applying a force per unit length $P = f\sqrt{3}/d$ on a hexagonal container with walls along the dense ball rows, as realized in [3]. The unit cell is defined by the two vectors $\mathbf{a}_{1,2} = d\hat{\mathbf{n}}_{1,2}$, the ball centers by $\mathbf{R}_{mn} = m\mathbf{a}_1 + n\mathbf{a}_2$.

One then obtains from Eqs. (5)–(8), for the vibrational modes of this system,

$$\mathbf{u}_{mn} = \mathbf{u} \exp_i[q \cdot \mathbf{R}_{mn} - \omega t], \quad \phi_{mn} = \phi \exp_i[(q \cdot \mathbf{R}_{mn} - \omega t)], \quad (9)$$

$$M\omega^2 \mathbf{u} = 2k \sum_{p=1}^{3} [1 - C_p(\mathbf{q})][(\mathbf{u} \cdot \hat{\mathbf{n}}_p)\hat{\mathbf{n}}_p + (\eta \mathbf{u} \cdot \hat{\mathbf{t}}_p)\hat{\mathbf{t}}_p]$$

$$+ i\eta k d \phi \sum_{p=1}^{3} S_p(\mathbf{q}) \hat{\mathbf{t}}_p, \quad (10)$$

$$I\omega^2 \phi = -i\eta k d \sum_{p=1}^{3} S_p(\mathbf{q})(\mathbf{u} \cdot \hat{\mathbf{t}}_p) + \eta k \frac{d^2}{2} \phi \sum_{p=1}^{3} [1 + C_p(\mathbf{q})], \quad (11)$$

where k is the normal stiffness common to all contacts and

$$S_p(\mathbf{q}) = \sin[d(\mathbf{q} \cdot \hat{\mathbf{n}}_p)], \quad C_p(\mathbf{q}) = \cos[d(\mathbf{q} \cdot \hat{\mathbf{n}}_p)], \quad (12)$$

and use has been made of relations such as $\Sigma_{p=1}^{6} \hat{\mathbf{n}}_p = 0$.

The exact spectrum in the full Brillouin zone, computed for $\mathbf{q}$ along two directions of high symmetry, is shown on Fig. 2. It can be inferred from these results that in this close-packed lattice the anisotropy of the spectrum is small.

In the elastic continuum, long wavelength limit $qd \ll 1$, decomposing the translation amplitude into its longitudinal and transverse components: $\mathbf{u} = u_{\parallel}\hat{\mathbf{q}} + u_{\perp}(\hat{\mathbf{z}} \times \hat{\mathbf{q}})$, one finds that the vibration spectrum, which is isotropic due to the hexagonal symmetry of the lattice, is composed of three branches.

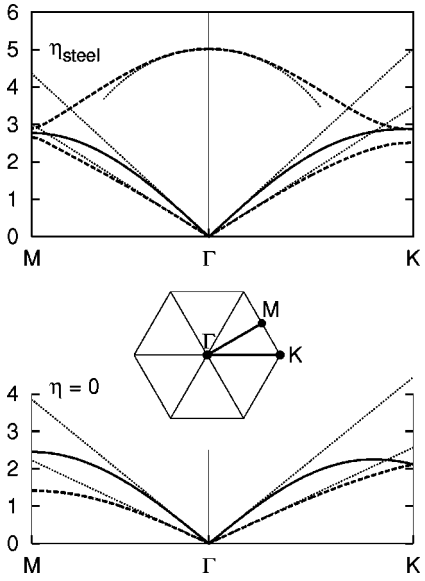

FIG. 2. Dimensionless dispersion curves for vibrations in the hcp lattice along two principal directions in the Brillouin zone. Units: $(k/M)^{1/2}$ for frequency, $2\pi/d$ for wave vector. Upper panel: frictional balls, $n_{\text{steel}} = 0.84$. Lower panel: frictionless balls. Middle: Brillouin zone, $\overline{\Gamma K} = \frac{2}{3} 2\pi/d$, $\overline{\Gamma M} = (1/\sqrt{3}) 2\pi/d$.

(i) Pure longitudinal acoustic modes of frequency $\omega_T = v_L q$, where the longitudinal sound velocity v_L is given by

$$v_L^2 = \frac{9}{8}\left(1 + \frac{\eta}{3}\right)\frac{k}{M} d^2. \quad (13)$$

(ii) Two branches of mixed modes containing both a transverse translational and a rotational component. One of them is acoustic: $\omega = v_T q$, where the transverse sound velocity reads

$$v_T^2 = \frac{3}{8}(1 + \eta)\frac{k}{M} d^2. \quad (14)$$

The second, which corresponds to pure rotation in the $q = 0$ limit, is an optical branch defined by

$$\omega_R^2 = 30\eta \frac{k}{M}(1 - \tfrac{1}{20} q^2 d^2). \quad (15)$$

That is, as already shown by Schwartz, Johnson, and Feng [15], the specificity of the vibration spectra of granular systems in frictional Hertz contact, as compared with atomic systems, lies in the additional degree of freedom associated with ball rotation. This remains coupled, in the long wavelength limit, with shear deformation, leading to a contribution $(-3\eta k d^2/4M)$ to v_T^2.

Also shown in Fig. 2 are the long wavelength dispersion curves. They can be seen to provide a good approximation for the exact spectrum in a sizeable fraction of the Brillouin zone.

It is worth recalling at this point that our equations of motion cease to be valid when the frequency approaches that of the lowest acoustic resonance of a ball: $\omega_{\text{res}} \approx v_{\text{bulk}}/d$,

with v_{bulk} being the sound velocity of the material constituting the balls. Indeed, in this situation, elastic deformations are no longer localized in a small region of extension of the order of the contact radius, internal deformations become important, and the restoring forces can no longer be described simply via the Hertz-Mindlin stiffnesses. Roughly speaking, this means that our expressions for the acoustic branches of the spectrum are valid provided that $v_{L,T} \ll v_{\mathrm{bulk}}$. In view of Eqs. (13), (14), and (2), this simply amounts to $(f/Ed^2)^{1/6} \ll 1$, which is realized under ordinary experimental conditions [16]. Note that this condition is equivalent to stating that the radius of the Hertz contact circle must be much smaller that the ball radius, which is precisely the condition for the Hertz approach to hold.

From planar continuum elasticity applied to a medium with hexagonal symmetry, the velocities of sound waves with propagation and polarization directions in the basal plane read

$$v_L^2 = \frac{K+G}{\tilde{\rho}} \quad v_T^2 = \frac{c}{\tilde{\rho}}, \tag{16}$$

where $\tilde{\rho}$ is the mass density of the medium, K and G are its bulk and shear moduli, respectively.

Comparison between these expressions and Eqs. (13) and (14) enables us to define elastic moduli for our ball lattice—a result that will be of use in the disordered case. They read

$$K = \frac{\sqrt{3}}{2}\frac{k}{d}, \quad G = \frac{(1+\eta)}{2}K, \tag{17}$$

where $\tilde{\rho}$ is related to the density of the ball material by $\tilde{\rho} = \pi\rho/3\sqrt{3}$.

III. DISORDERED LATTICE

A. Random hcp array of balls under hydrostatic compression

Consider an ensemble of balls whose material parameters are identical, while their diameters vary at random with a continuous or discrete statistical distribution. A diameter value d^Q, with a formal label Q, has the probability or fractional concentration c^Q and $\Sigma c^Q = 1$.

The mean diameter d of a set of $N \gg 1$ such balls may be obtained by configuration average, which we will denote by $\langle \cdots \rangle$

$$d = \frac{1}{N}\sum_i d_i \to d \equiv \langle d \rangle = \sum_Q c^Q d^Q. \tag{18}$$

We define the random deviations by

$$\Delta_i = d_i - d, \quad \Delta^Q = d^Q - d,$$

$$(\Delta) = 0, \quad \Delta_{\mathrm{RMS}}^2 \equiv \langle \Delta^2 \rangle = \sum c^Q (\Delta^Q)^2. \tag{19}$$

In actual computations, we will use the uniform distribution with full width $W = \max\{\Delta^Q\} - \min\{\Delta^Q\}$, which means $\Delta_{\mathrm{RMS}} = W\sqrt{12}$.

One sample (configuration) of the random hcp array of balls may be created by randomly distributing the balls in an uncorrelated way over the sites of a reference hcp lattice. The number of balls is assumed to be sufficiently large for the thermodynamic limit to be approached. The sample is then random but macroscopically homogeneous. The balls are brought into contact and further compressed by external compressive forces applied to the sample boundaries so that the average internal stress is hydrostatic. An easy way of achieving this is to assume a hexagon shaped sample and to apply to all its sides the same macroscopic pressure force. The pressure force per unit length P will be henceforth called *linear pressure*. Under this pressure, the size of the compressed sample is reduced, while the symmetry of the lattice is preserved on average. It is thus meaningful to introduce an *average lattice spacing a* as a macroscopic parameter having a thermodynamic limit and globally characterizing the state of the sample.

The pressure and the size of the compressed system are related by the *macroscopic equation of state* for the random lattice under hydrostatic compression. It will be convenient to introduce it in the form

$$f = \tilde{f}(a), \quad f = Pd/\sqrt{3}, \tag{20}$$

where $\tilde{f}$ is the functional dependence in question and f denotes the *average intergrain hydrostatic force* associated with the linear pressure P. The *effective normal stiffness* $\tilde{k}$ and the effective bulk modulus K_{eff} are then given by

$$\tilde{k}(a) = -\frac{d\tilde{f}(a)}{da}, \quad K_{\mathrm{EFF}} d = -\frac{a^2}{\left(\frac{da^2}{dP}\right)} = \frac{\sqrt{3}}{2}\tilde{k}. \tag{21}$$

As for the d factor on the left-hand side, cf. Eq. (17).

While the global characteristics P and a have thermodynamic limits, the ball positions and contact forces are subject to pronounced fluctuations, in particular for small external loads. In experiments, this double nature of the disordered state is manifested by the coexistence of coherent signals and irregular speckles in the acoustic response [3,17], in numerical simulations most clearly by the formation of force chains [7,18].

Let us first verify that the geometrical disorder can be taken as small, as demanded in Sec. II A. If the relative diameter spread is small, the equilibrium disordered system can be treated, for any external pressure, as a distorted lattice. The balls are slightly displaced, and, in the case of frictional balls, the contact points may be somewhat off the intercenter lines, which gives rise to non-normal contact forces. Taking as representative the data of [3], $W \lesssim 8\ \mu$m, $d = 8$ mm for steel balls, we see that the relative dispersion in ''bond'' lengths is of the order of 10^{-3}. By geometrical considerations, this corresponds to deviations of the direction of the contact force from the normal also of about 10^{-3} rad. These figures indicate that the geometrical disorder in this case is small indeed.

Fluctuations in the magnitude of the random contact forces, by contrast, may be quite large. From Eq. (1), the contact force as a function of intercenter distance is given by

$$f_{ij}(x)=\begin{cases} \frac{2}{3}E^*\underbrace{(d_{ij}^*)}_{\approx d}{}^{1/2}(d_{ij}-x)^{3/2}, & d_{ij}-x>0 \\ 0, & d_{ij}-x<0. \end{cases} \tag{22}$$

As indicated by the underbrace in Eq. (22), it is consistent to neglect the randomness of d_{ij}^*. Namely, the fractional fluctuation of $d_{ij}^*\approx d+\frac{1}{2}(\Delta_i+\Delta_j)$ is $\sim\Delta_{\mathrm{RMS}}/d$.

On the other hand, the disorder of the last factor in Eq. (22) is crucial: for the Hertz displacement $d_{ij}-x$, the ratio $\Delta_{\mathrm{RMS}}/(d-x)$ may be large or small depending on the degree of compression of the balls, while both basic conditions. $\Delta_{\mathrm{RMS}}\ll d$ (small disorder) and $d-x\ll d$ (Hertz picture), remain satisfied. We may thus envisage three different regimes.

Regime	Condition
Low pressure	$\Delta_{\mathrm{RMS}}\gg d-x$
Intermediate pressure	$\Delta_{\mathrm{RMS}}\approx d-x$
High pressure	$\Delta_{\mathrm{RMS}}\ll d-x$

In the high-pressure Hertz regime, $\Delta_{\mathrm{RMS}}\ll d-x\ll d$, the disorder appears as a perturbation of a basic homogeneous and homogeneously compressed crystal. This natural conjecture has given rise to two simple, but useful approximations (see [7]) for the true effective medium.

(i) The *averaged lattice approximation* (ALA) replaces the true sample by an ideal lattice of balls with the diameter d. The constitutive law and the bulk modulus thus read [19]

$$\tilde{f}(a)=\tfrac{2}{3}E^*d^{1/2}(d-a)_+^{3/2}\equiv F(a), \tag{23}$$

$$K_{\mathrm{ALA}}=E^*\left(\frac{9}{16}\frac{P}{E^*d}\right)^{1/3}. \tag{24}$$

Thus, the bulk modulus naturally obeys the plain Hertz $\frac{1}{3}$ law, as is appropriate for a periodic array (see Sec. II).

(ii) The *averaged force approximation* (AFA) assumes the balls to be positioned at any pressure exactly at the lattice sites, while the contact forces are given by Eq. (22). In this strictly symmetric geometry, no shear forces between the grains occur, and the effective hydrostatic force between two adjacent sites is obtained by configuration averaging,

$$\tilde{f}(a)=\langle f_{ij}(a)\rangle\equiv F_{\mathrm{av}}(a),$$

$$F_{\mathrm{av}}(a)=\sum_{Q,Q'}c^Qc^{Q'}F^{QQ'}(a), \tag{25}$$

where we have introduced the notation

$$F^{QQ'}(x)=\tfrac{2}{3}E^*d^{1/2}(d^{QQ'}-x)_+^{3/2}. \tag{25a}$$

for a force at a separation x between two balls of the prescribed species Q, Q' with $d^{QQ'}=\frac{1}{2}(d^Q+d^{Q'})=d+\Delta^{QQ'}$. Asymptotically,

$$\tilde{f}(a)\sim F(a)\left(1+\frac{3}{8}\frac{\Delta_{\mathrm{RMS}}^2}{(d-a)^2}\right) \tag{26}$$

and the bulk modulus becomes

$$K_{\mathrm{AFA}}=K_{\mathrm{ALA}}\left(1-\frac{1}{8}\frac{\Delta_{\mathrm{RMS}}^2(\frac{4}{3}E^{*2}d^{-1})^{2/3}}{P^{4/3}}\right). \tag{27}$$

These two equations show that the AFA effective contacts are non-Hertzian, and that the pressure dependence of the elastic modulus deviates from the simple $\frac{1}{3}$ power law.

While the ALA has an arbitrary nature, the AFA seems to be justified for high pressures, when the geometrical disorder is small compared to the compressive displacements, while the contact forces still continue to exhibit random fluctuations. These force fluctuations then appear as being responsible for the non-Hertzian features of the effective contacts [20].

At lower, ''intermediate,'' pressures, according to our above classification, all grains are still mutually engaged through their contacts, but the random displacements become comparable to the global compressive deformations. The AFA is then not sufficient, while an approximation taking these local lattice distortions into account in an averaged manner may be satisfactory. The effective medium approximation (EMA) described in the next section is an attempt in this direction.

B. Effective medium approximation

Now, we are ready to build our effective medium approximation for the disordered hexagonal array of balls. We use this name, conventional in the context of granular assemblies, but as sketched already in the Introduction, a more descriptive name would refer to the mean-field nature of the approximation, or, alternatively, to its ''single-site'' character. The universal idea of such approximations is as follows [11]. We will only consider disordered systems in which a periodic geometrical lattice (2D hcp in our case) is filled by elementary objects associated with individual sites (balls for us) and having randomly variable characteristics (radii). It is assumed that the macroscopic properties of such random systems can be obtained, in principle, by configuration averaging. The configurationally averaged system is exactly periodic again. In the mean-field approximation, one assumes that it can be represented as a periodic array of effective elementary objects similar in nature to the random elements of the real array. The characteristics of these are determined by the following self-consistent procedure. One of the effective elements is replaced back (substituted) by a true random one. The new system is locally sampled in a random fashion. It is then required that a configuration average of these locally distorted systems restores the average behavior. This

condition determines the characteristics of the effective elements. Once this has been done, the whole task of configuration averaging is complete.

An effective medium theory along these lines was developed by Feng and co-workers in [12,13] to study depleted elastic networks on lattices. The basic element in the theory of these authors was a single bond connecting two lattice sites. The bonds were described by their linear stiffnesses, whose random distribution was prescribed *a priori*. The resulting EMA [a single-bond CPA] provided a theory for the effective linear elasticity of the network, and for its vibrational spectrum.

While this bond EMA was a successful theory in its own area, we contend that it cannot be used for random Hertz lattices for two essential reasons.

(i) The elementary object in a granular system is a ball. The star of (six for 2D hcp) contacts surrounding the ball, that is, of ''bonds'' stemming from the center, is statistically correlated, and the bonds cannot be treated as independent.

(ii) The linear stiffnesses of the contacts are not known beforehand. They are indirectly specified by the average external pressure, but their local fluctuations depend on the equilibrium ball positions and cannot be determined independently of the nonlinear static equilibration of the Hertz array at a given pressure.

These two points are of a different nature and importance. The second point holds for any granular system, and we believe that it is precisely this that has been the obstacle against developing a satisfactory EMA for the acoustic response of granular materials. It may be said that the grain network should fulfill two contradicting roles at the same time, namely, it should constitute the medium for wave propagation as well as the random scattering field. We will see how this basic problem can be overcome in our rather specifically constructed case.

1. EMA for frictionless balls

To develop an EMA incorporating these features, we consider first the case of nonfrictional Hertz contacts (formally, $\eta=0$). The averaged array is assumed to consist of *effective balls* whose diameter is a. The principal assumption is that the average hydrostatic force $\tilde{f}(a)$ can be interpreted locally as a contact force between two effective balls, so that $\tilde{k}(a)=-(d/da)\tilde{f}(a)$ is the stiffness of an effective contact between two such balls. Now, we select one site, ''0,'' as central and substitute a ball with diameter d^Q for the effective ball. The difference d^Q-a in diameters will give rise to an elastic deformation of the effective lattice. In other words, the substituted ball acts as an elastic inclusion. On average, the deformation should cancel. This would define the EMA condition, if only we were able to determine the force between a real and an effective ball. This is not possible directly, and we propose to overcome this by considering a cluster consisting of the central ball and a ''corona'' of its nearest neighbors as sketched in Fig. 3. These neighbors have a hybrid nature. In other words, the interface between the effective medium and the inclusion passes through the corona balls. All contacts between the corona balls and the adjacent effective balls are taken as effective ones, associated with the force $\tilde{f}$. This type of approximation is based on the mean-field reasoning: the fluctuations of the remote parts of the lattice should not have a significant effect on the central site.

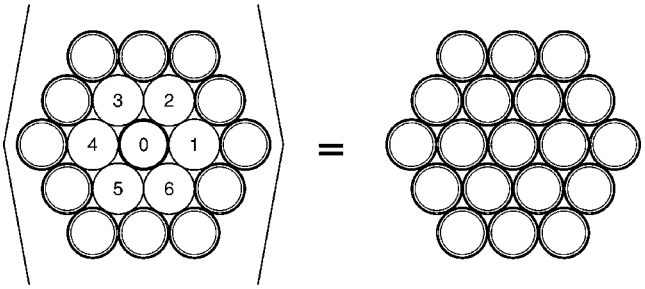

FIG. 3. Graphical representation of the EMA averaging process. On the left, a cluster (central ball 0 surrounded by its corona, balls 1–6) embedded in the effective medium. Configuration averaging $\langle\cdots\rangle$ restores the effective medium on the right.

Inside the cluster, the corona balls might appear as ''true'' randomly chosen balls, so that the contact forces would be of the form $F^{QQ'}$ as given by Eq. (25a). A straightforward procedure involving averaging over the individually equilibrated positions of such randomly composed clusters of seven balls, while conceivable, would be disproportionately clumsy.

We prefer to introduce a model of the *corona*, which, while simple and transparent, captures the core features of the problem.

(1) The contact forces between the central ball and the corona balls are averaged over the corona configurations,

$$f_{0i}(x)\to F^Q(x)\equiv\sum_{Q'} c^{Q'}F^{QQ'}(x),\quad i=1\div 6. \tag{28}$$

These forces incorporate in full the symmetric, radial fluctuations caused by the randomness of the central ball, while all angular correlations are averaged over and the forces have full hexagonal symmetry.

(2) The contact forces between the touching corona balls are assumed to be given by the effective force law $\tilde{f}(x)$.

The displacements of the corona balls are then also symmetric. This restores the basic picture of a symmetric inclusion in the effective lattice. The central ball remains at its site, while the corona breathes around it symmetrically in accordance with the central site occupancy and transfers this to an equilibrium symmetric distortion of the surrounding effective lattice.

Returning to Fig. 3, we see that the cluster is surrounded by 12 effective balls forming a hexagon. They are of two kinds: six occupy the corners (''on-top'' positions with respect to the corona balls) and another six sit along the edges (''bridge'' positions). The displacement field around the ''1'' ligand is sketched in Fig. 4. The scalar u is the radial displacement common to all corona balls, u_α and u_β correspond to the on-top and bridge neighbors, respectively. The arrows

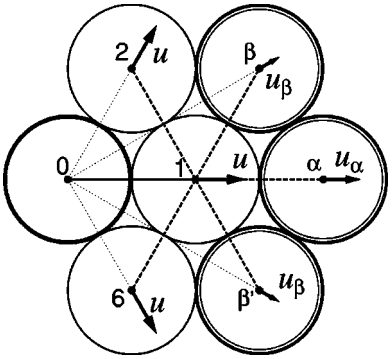

FIG. 4. Displacements of the neighbors of the cluster central ball 0. Corona balls: 1, 2, 6. Second neighbors: effective balls in the on-top (α) and bridge (β and β') positions.

indicate the directions of the displacements, whose magnitude varies with the Q label of the central ball, and should be labeled u^Q, u_1^Q,... .

Ball 1 is acted upon by contact forces from all its neighbors. The force coming from the central ball is random [Eq. (28)],

$$\mathbf{f}_{01}=F^Q(a+u^Q)\hat{\mathbf{n}}_1. \tag{29}$$

In the regime of small displacements ($\sim$ high pressures), we may expand

$$\mathbf{f}_{01}=[F^Q(a)-K^Q(a)u^Q]\hat{\mathbf{n}}_1, \quad K^Q(x)=-\frac{d}{dx}F^Q(x). \tag{30}$$

The remaining five forces are given by the effective interaction $\tilde{f}$. They are of three types. In the regime of small displacements, we obtain [cf. Eq. (5)]

$$\mathbf{f}_{\alpha 1}=\tilde{f}(a)\hat{\mathbf{n}}_4-\tilde{k}(a)(u^Q-u_\alpha^Q)\hat{\mathbf{n}}_4,$$

$$\mathbf{f}_{\beta 1}=\tilde{f}(a)\hat{\mathbf{n}}_5-\tilde{k}(a)\left[\left\{u^Q\hat{\mathbf{n}}_1-u_\beta^Q\frac{1}{\sqrt{3}}(\hat{\mathbf{n}}_1+\hat{\mathbf{n}}_2)\right\}\cdot\hat{\mathbf{n}}_2\right]\hat{\mathbf{n}}_2,$$

$$\mathbf{f}_{21},\ldots=\tilde{f}(a)\hat{\mathbf{n}}_3-\tilde{k}(a)u^Q\hat{\mathbf{n}}_3. \tag{31}$$

The forces depend on the three displacements u^Q, u_α^Q, u_β^Q. In the linear elasticity regime corresponding to our assumption of small displacements, a simple universal relation exists between these three displacements,

$$u_0=\alpha u, \quad u_\beta=\beta u, \tag{32}$$

where α and β are geometrical parameters independent of the magnitude of u. They can be determined for a linear elastic array of nonfrictional balls once for ever, although not in a closed analytic form. Details of the calculation of both parameters are in the Appendix. The resulting values are

$$\alpha=0.585\,405$$

$$\beta=0.232\,971$$

Now, we require that *the total equilibrium force on ball 1 vanishes*, and subtract from this condition the equilibrium condition for the effective lattice

$$\mathbf{f}_{01}+\mathbf{f}_{61}+\mathbf{f}_{\beta 1}+\mathbf{f}_{\alpha 1}+\mathbf{f}_{\beta' 1}+\mathbf{f}_{21}=0,$$

$$\tilde{f}(a)\{\hat{\mathbf{n}}_1+\hat{\mathbf{n}}_2+\hat{\mathbf{n}}_3+\hat{\mathbf{n}}_4+\hat{\mathbf{n}}_5+\hat{\mathbf{n}}_6\}=0. \tag{33}$$

Only the component parallel to the 01 connecting line is nontrivial. With the help of Eq. (31) it reduces to a single equation for a single unknown, the corona radial displacement, with the solution

$$u^Q=\frac{F^Q(a)-\tilde{f}(a)}{K^Q(a)+\Xi\tilde{k}(a)}, \tag{34}$$

where

$$\Xi=\frac{5}{2}-\alpha-\beta\frac{\sqrt{3}}{2} \tag{35}$$

is again a geometrical factor. The equation has a simple interpretation. For a given Q, the difference between the force exerted by the inclusion and the average force gives rise to a radial displacement. Its magnitude is related to the force by an *additively renormalized stiffness* reflecting the fact that the corona is supported by the rest of the (effective) lattice. In the mean-field context, this renormalization is a *local field correction*, and the parameter Ξ measures its dimensionless strength.

Now, we may impose the self-consistency condition, requiring that the average displacement be zero,

$$\langle u^Q\rangle=\sum_Q c^Q\frac{F^Q-\tilde{f}}{K^Q+\Xi\tilde{k}}=0, \tag{36}$$

where the argument of all functions is a. This single implicit equation links the corona radial displacement with the unknown $\tilde{f}$. It can be rearranged into a suitable explicit form. First, introduce

$$F_{\rm av}=\langle F^Q\rangle=\sum_Q c^Q F^Q,$$

$$\frac{1}{K^*}=\sum_Q c^Q\frac{1}{K^Q+\Xi\tilde{k}}. \tag{37}$$

$F_{\rm av}$ is easily recognized as the averaged force of the AFA [Eq. (25)] K^* is an averaged radial stiffness of the lattice surrounding a single ball inclusion. Writing $F^Q-\tilde{f}=(F^Q-F_{\rm av})+(F_{\rm av}-\tilde{f})$ and using Eq. (37), we bring the EMA condition (36) to the form

$$\tilde{f}=F_{\rm av}+K^*\sum_Q c^Q\left(\frac{1}{K^Q+\Xi\tilde{k}}-\frac{1}{K^*}\right)(F^Q-F_{\rm av}). \tag{38}$$

The average hydrostatic force $\tilde{f}$ for a given lattice spacing is seen to contain two contributions. First, the nonselfconsistent averaged contact force, and, second, a term having the characteristic structure of a correlator involving self-consistent fluctuations of two random variables. This form is known from CPA-like theories. We have to refer to Ref. [11] for the original CPA for electrons in alloys, but here we contrast (36) with the bond CPA of Refs. [12,13]. Their CPA for an effective stiffness of a depleted elastic network had the same overall form, but it was an algebraic equation, because the stiffnesses of the bonds were taken as known and the force whose derivative determines the stiffness did not enter the equations. In our case, we have to consider the forces and the stiffnesses simultaneously, and the second term of Eq. (38) is responsible for the peculiar character of the self-consistency. It is not the unknown $\tilde{f}$ itself that appears on its right-hand side, but its derivative $\tilde{k}(a)=-(d/da)\tilde{f}(a)$, so that Eq. (38) has the form

$$\tilde{f}(a)=F_{\mathrm{av}}(a)+\mathcal{F}\left(\Xi\left|a,\frac{d}{da}\tilde{f}(a)\right.\right), \tag{39}$$

where $\mathcal{F}$ is a complicated but well-defined function. The EMA equation is thus a first-order differential equation determining $\tilde{f}$ as a function of a. In other words, we have here a case where self-consistency cannot be written directly for an isolated value of the control parameter a, but involves intrinsically the whole functional dependence $\tilde{f}(a)$. This is a physical rather than a formal feature of the theory due to the nonlinearity of the Hertz forces and stiffnesses [see Eq. (2)]. The notion of an incremental buildup of stress was introduced in [2] for general Hertz-Mindlin granular systems. Our system is special in that it remains elastic. On the other hand, local distortions in the random ball arrangements depend on the global evolution of the system and cannot be obtained but via an incremental process, of which the EMA equation (39) is the mean-field representation [21].

To select the physically relevant solution of Eq. (39), we rely upon the high-pressure asymptotic boundary condition

$$\tilde{f}(a)\sim F_{\mathrm{av}}(a) \qquad \text{for} \quad \Delta_{\mathrm{RMN}}\ll d-a \quad (\ll d). \tag{40}$$

It can be explicitly verified from Eq. (38) that the contact of $\tilde{f}$ with F_{av} stipulated by Eq. (40) is of second order, so that the boundary condition is formally justified. Physically, this condition means that the EMA coincides with the AFA in the asymptotic limit of high pressures, but extends the mean-field description of the system to an intermediate-pressure region. We may also say that our EMA is a self-consistent resummation of the high-pressure perturbation expansion for the equation of state $\tilde{f}(a)$.

The solution of the EMA equation (39) is obtained without difficulty by numerical iteration starting from $\tilde{f}^{(0)}(a)=F_{\mathrm{av}}(a)$.

2. EMA for frictional balls

The case of frictional balls is very important for a proper comparison with existing experimental data. A formal development of the EMA for frictional balls can proceed quickly, because the steps are almost identical with those made for the nonfrictional case. It is necessary, however, to extend the description of the effective medium. As before, it is assumed to be composed of effective balls with diameter a, interacting through effective contacts. In addition to the average hydrostatic force $\tilde{f}$ and the normal stiffness $\tilde{k}=-(d/da)\tilde{f}(a)$, we have to postulate also a local shear (tangential) stiffness $\tilde{\kappa}$ as a third basic characteristic of the effective contact. For $\tilde{\kappa}$, we formulate our basic conjecture

$$\tilde{\kappa}=\eta\tilde{k}. \tag{41}$$

In words, the effective shear and compressive stiffnesses are related in the same manner as the two stiffnesses for actual Hertz-Mindlin contacts; in Eq. (4), η is introduced as their ratio and expressed in terms of the bulk Poisson ratio σ alone. This independence of η on the local geometry and forces supports the above ansatz. It is justified within the AFA, that is, in an asymptotic sense. We will further discuss this intuitively appealing conjecture below, but first derive the EMA equations following the preceding paragraph step by step.

The central ball inclusion and its symmetrized corona are introduced without changes and both Figs. 3 and 4 remain valid. Due to the symmetry of the cluster, there is no torque acting on either the central or the corona balls and only the force equilibrium has to be considered. The central ball is equilibrated automatically, and we inspect the forces acting on the corona ball 1, linearized again with respect to the small displacements. The full expression (5) must be used now. The relative displacements remain radial for all the neighbors of ball 1, except for the β and β' ones (see Fig. 4). For β's, the contact force has a shear component.

$$\mathbf{f}_{\beta 1}=\tilde{f}(a)\hat{\mathbf{n}}_5-\tilde{k}(a)\left[\left\{u^Q\hat{\mathbf{n}}_1-u^Q_\beta\frac{1}{\sqrt{3}}(\hat{\mathbf{n}}_1+\hat{\mathbf{n}}_2)\right\}\cdot\hat{\mathbf{n}}_2\right]\hat{\mathbf{n}}_2-\tilde{\kappa}(a)$$
$$\times\left[\left\{u^Q\hat{\mathbf{n}}_1-u^Q_\beta\frac{1}{\sqrt{3}}(\hat{\mathbf{n}}_1+\hat{\mathbf{n}}_2)\right\}\cdot\hat{\mathbf{t}}_2\right]\hat{\mathbf{t}}_2 \tag{42}$$

and similarly for β'. Finally, the displacements u^Q, u^Q_α, u^Q_β obey, in the linear elasticity regime, universal relations similar to Eq. (32),

$$u_\alpha=\alpha(\eta)u, \quad u_\beta=\beta(\eta)u, \tag{43}$$

where the α and β parameters depend now on the stiffness ratio η, as indicated.

Introducing Eqs. (41)–(43) into the equilibrium condition (33), which is fully general, we obtain the corona radial displacement as

$$u^Q=\frac{F^Q(a)-\tilde{f}(a)}{K^Q(a)+\Xi_\eta\tilde{k}(a)}, \tag{44}$$

in complete analogy with the frictionless case, Eq. (34). The only change is an η-dependent geometrical factor, which reads now

$$\Xi_\eta = \frac{5}{2} - \alpha(\eta) - \beta(\eta)\frac{\sqrt{3}}{2} + \eta\left[\frac{3}{2} - \beta(\eta)\frac{\sqrt{3}}{2}\right]. \quad (45)$$

The EMA condition $\langle u^Q \rangle = 0$, Eq. (36), has a universal character, and with u^Q given by Eq. (44), it can be brought successively to various explicit forms following strictly Eqs. (36)–(39), with Ξ of Eq. (35) replaced everywhere by Ξ_η as given by Eq. (45). For convenience, we present here the final form of the EMA,

$$\tilde{f}(a) = F_{\rm av}(a) + \mathcal{F}\left(\Xi_\eta \middle| a, \frac{d}{da}\tilde{f}(a)\right) \quad (46)$$

The corresponding boundary condition (40) is η independent. The two complementary cases, frictional and nonfrictional, are thus given by the same differential equation with the same boundary condition. They are only distinguished by the value of the Ξ_η parameter, which corresponds to $\eta \neq 0$ and $\eta = 0$, respectively. In other words, the difference between the two physical situations is reflected in the EMA through the strength of the local field correction appearing in the renormalized contact stiffness.

C. Macroscopic properties in the EMA

To complete the EMA analysis of our granular system, let us now derive the expressions for the sound velocities. Macroscopically, the averaged system is a periodic hcp structure, so that it is acoustically isotropic and there exist just two sound velocities v_L and v_T, as in the ideal lattice of Sec. II B. There, we proceeded from the full dispersion law in the Brillouin zone to the long wavelength limit [Eqs. (13) and (14)], then to the elastic moduli (17) on the basis of the macroscopic (continuum) relations (16).

For the disordered system, we shall go in the reverse direction. The EMA yields directly the equation of state $\tilde{f}(a)$ and the effective compressive stiffness $\tilde{k}(a)$. The equation of state is a monotonic function of a and thus can be inverted into $\tilde{a}(f)$. Using Eq. (20), we obtain finally the average lattice spacing as a function of the linear pressure P and any function of a, such as the bulk modulus, can be converted into a function of the pressure.

The bulk modulus is obtained from the stiffness $\tilde{k}$ using Eq. (21). It should be stressed that Eqs. (17) and (21) have an identical form; in fact, Eq. (17) as far as it concerns the bulk modulus is but a special case of Eq. (21) for zero disorder. As concerns the shear modulus, since our method only allows for treating the effect of hydrostatic stresses, we resort to an ansatz, i.e., we propose to extend relation (17) for G to the disordered case. We then get

$$K_{\rm eff} = \frac{\sqrt{3}}{2}\frac{\tilde{k}}{d}, \quad G_{\rm eff} = \frac{(1+\eta)}{2}K_{\rm eff}. \quad (47)$$

While the first relation is exact, we should discuss the meaning of the second one. It turns out that the equivalent relation (17) for the ideal array is a direct consequence of the Mindlin ratio (6) between near-normal stiffnesses and does not depend on the specific value or character of the compressive stiffness. Thus, the second of Eqs. (47) is in fact equivalent to our conjecture (41) about the ratio of effective stiffnesses, $\tilde{\kappa} = \eta\tilde{k}$. Once the effective moduli are known, the sound velocities become

$$v_L^2 = \frac{K_{\rm eff} + G_{\rm eff}}{\tilde{\rho}}, \quad v_T^2 = \frac{G_{\rm eff}}{\tilde{\rho}}. \quad (48)$$

Equations (47) then predict for the velocity ratio that

$$\frac{v_L^2}{v_T^2} = \frac{3+\eta}{1+\eta}. \quad (49)$$

This is a very strong prediction, according to which the velocity ratio should depend neither on the pressure nor on the disorder level, being fully determined by the material properties of the grains. While Eq. (41) is not susceptible of direct verification, the predicted sound velocity ratio can be tested for a wide range of systems. Note that a similar conjecture concerning this ratio was formulated earlier by Schwartz, Johnson, and Feng [15].

In order to avoid resorting to such a guess, one would have to develop an extended EMA yielding both moduli $K_{\rm eff}, G_{\rm eff}$ directly by considering also a macroscopic shear.

IV. DISCUSSION

We first confront our mean-field predictions with the experimental data obtained by Gilles and Coste [3], on an hcp lattice of steel balls confined by a hexagonal frame under hydrostatic loading. They measured the time of flight of a low frequency sound pulse between two opposite sides of the frame. From this we obtain the longitudinal sound velocity $v_L(f)$, where f is the average equilibrium contact force, Eq. (20).

The experimental data show that at the highest loadings used, v_L approaches closely the $P^{1/6}$ Hertz behavior. This confirms that, in this regime, the applied pressure is high enough for disorder effects to be weak, and for the compressed lattice to be close to the ideal hcp one.

We, therefore, focus first on the data for the largest forces used in the experiments. For example, an external force of $\sim$990 N applied on each side of a hexagon with 31 balls in contact with each side corresponds to $f = 18.446$ N. Taking for steel $E = 9.20 \times 10^{10}$ Pa, $\sigma = 0.276$, $\rho = 7840\ \mathrm{kg\,m^{-3}}$, ball diameters $d = 8$ mm, we get from Eqs. (2), (3), and (13) $v_L = 791\ \mathrm{m\,sec^{-1}}$, to be compared with the experimental value of $778\ \mathrm{m\,sec^{-1}}$. The agreement is seen to be excellent, to the precision of the numerical input.

Note that the contribution of the tangential contact stiffness is non-negligible: with the above value of σ, the Mindlin coefficient $\eta = 0.84$. Neglecting the frictional character of the contacts ($\eta = 0$) leads to underestimating the longitudinal velocity by $\approx$11%, well out of the experimental error bar.

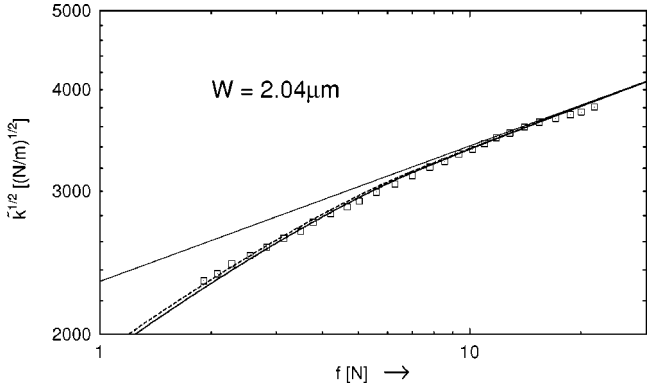

FIG. 5. Square root of effective compressive stiffness vs effective contact force. Squares: experiment (Ref. [3]). Thick line: EMA for frictional balls. Dashed line: EMA for frictionless balls. Thin line: ALA (ideal Hertz dependence).

For the transverse velocity, the two values would differ by $\approx$35%, but no experimental data are available. These differences in velocities are clearly reflected in the different slopes of the dispersion curves for the frictional and nonfrictional cases in Fig. 2.

With the values of v_L at hand, we may return to the discussion at the end of Sec. II B and check first the validity of the Hertz approach. The bulk sound velocities for the above material parameters of steel are $v_{L,\mathrm{bulk}}=5825\,\mathrm{m\,sec}^{-1}$, $v_{T,\mathrm{bulk}}=3252\,\mathrm{m\,sec}^{-1}$ and we may conclude that the condition $v_{L,T}\ll v_{L,T,\mathrm{bulk}}$ is obeyed. To verify the validity of the continuum limit, we have to invoke the ground frequency of the pulses used in the experiments, $\omega=2\pi\times6500$ Hz. This yields $q(2\pi/d)^{-1}\approx0.066$, much less than 1 indeed. Expressed in terms of wavelengths, $\lambda\approx0.122\,\mathrm{m}\sim15d$. These estimates made for one pressure may be taken as representative for the whole experimental pressure range, as the experimental velocities vary between 500 and 800 $\mathrm{m\,sec}^{-1}$.

In order to analyze the pressure dependence, we deduce from the v_L data the effective normal stiffness $\tilde{k}$ with the help of Eqs. (49) and (48), assuming frictional contacts with $\eta=0.84$. It is plotted on Fig. 5. It is clearly seen that the high-pressure data fit the straight line corresponding to the ideal lattice. As f decreases, the logarithmic slope increases, coming close to the popular $\nu\approx\frac{1}{4}$ value. However, no sharp crossover is identifiable, the transition being completely smooth.

We then solve the mean-field equation numerically. All parameters are known, except for the width of the distribution of ball diameters. Diameter scatter is only qualified, in the experiment, through a tolerance of ±4 μm. We assume a uniform distribution whose width W is our single fitting parameter. We find that the best fit is obtained for $W=2.04$ μm, completely compatible with the tolerance figure. The fit itself is seen to be very good in the whole experimental range. The EMA is shown both for frictional and nonfrictional balls. The results are only weakly sensitive to the value of η, at striking variance with the sound velocity itself. For the latter quantity, however, the η dependence enters primarily through the $G_{\mathrm{eff}}/K_{\mathrm{eff}}$ ratio.

The experimental f range is limited, on the low force side, to $f\simeq2$ N. Furthermore, no direct measurement of the equation of state $\tilde{f}(a)$ is available yet. It is, therefore, of great interest to complement the above comparison with a confrontation between mean-field predictions and the simulations performed by Roux [7] on the same system for frictionless balls with a uniform random distribution of diameters. Applied forces span the whole range from almost zero up to the upper experimental limit. The comparison for the equation of state is shown in Fig. 6, which is drawn in the dimensionless representation used in Ref. [7],

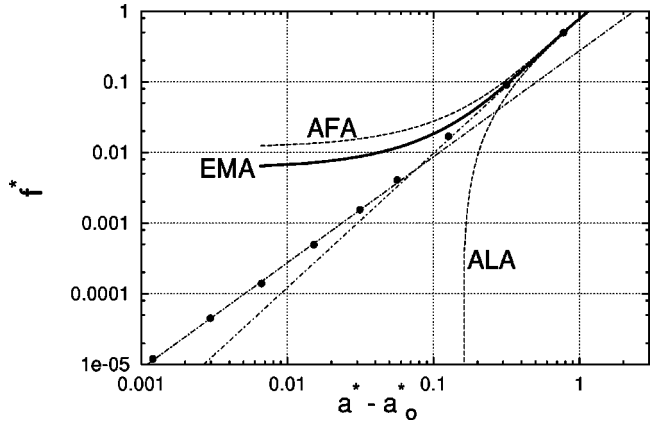

FIG. 6. Effective force vs displacement in dimensionless units (see text) for frictionless balls. a_0^* corresponds to the rigidity threshold. Dots: numerical results. Dash-dotted lines: power law approximants of numerical results (Ref. [7]).

$$a^*=\frac{d+\frac{1}{2}W-a}{W},\quad f^*=\frac{f}{\frac{2}{3}E^*d^{1/2}W^{3/2}}.$$

In these units, the exact equation of state $f^*(a^*)$ is a universal function [7] if approximation (22) is used. It is easy to verify on Eq. (38) that the EMA has the same property.

Clearly, $a^*\geqslant0$. For $a^*=0$, the balls barely start touching, $a_0^*=0.343$ is the so-called rigidity threshold, below which the disordered lattice cannot sustain compression $a^*\geqslant1$ is

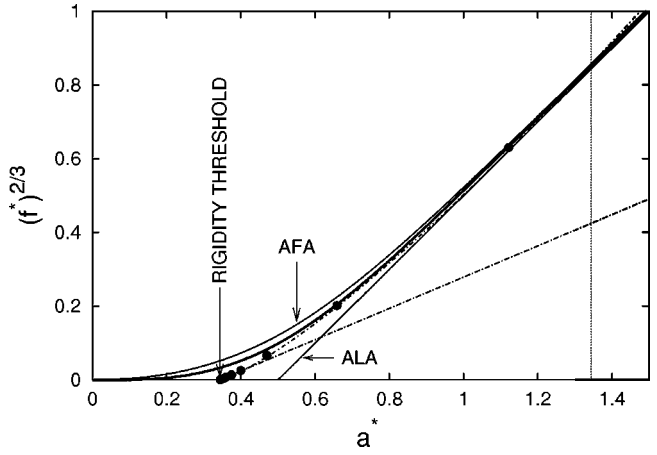

FIG. 7. Effective force vs displacement in the ''Hertz'' representation. Data and symbols as in Fig. 6.

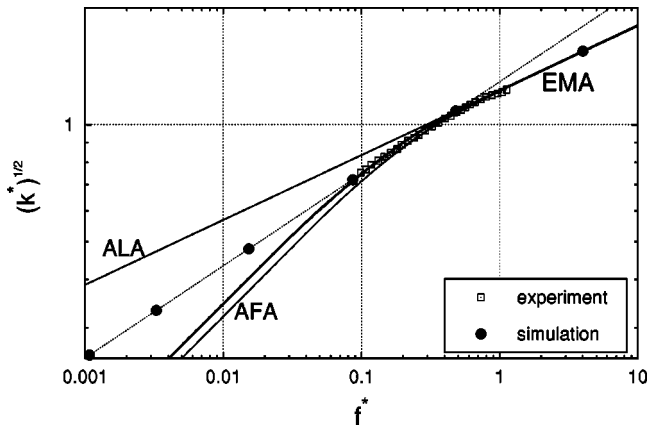

FIG. 8. Square root of effective compressive stiffness vs effective contact force (dimensionless units).

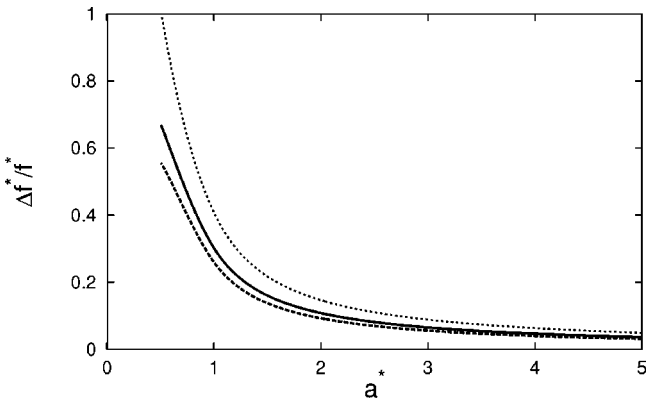

FIG. 9. Relative fluctuation of local contact force vs dimensionless displacement. Full line: EMA for frictional balls. Thick dashed line: EMA for frictionless balls. Dotted line: AFA.

the region where all neighbors are already in contact, and $a^* \gg 1$ is the high-pressure limit. In a narrow range above the rigidity threshold, a quasi-Hertz regime is found followed, in the intermediate force range, by a steeper variation. The mean-field result shown here, also calculated for frictionless balls, appears to agree with the numerical data for $(a^* - a_0^*) \gtrsim 0.3$. Also shown are the curves corresponding to the ALA and to the AFA. They frame the exact and the EMA results from below and from above, respectively. For high pressures, all plots merge. We replot the same data in Fig. 7 using the linear scale for the lattice spacing and the $\frac{2}{3}$ power scale for the forces, so that the natural range of various regimes can be better assessed. In particular, note the striking improvement of EMA over the AFA for intermediate pressures.

In Fig. 8 we return to the experimentally more relevant stiffness-force dependence and plot in dimensionless form the mean-field and the ALA curves, the data from Roux's numerical simulations and their power law approximants, and also the experimental data of Gilles and Coste. These data are scaled using $W = 2.04\,\mu$m and the force unit $\frac{2}{3}E^* d^{1/2} W^{3/2} = 19.89$ N. The overall agreement is truly satisfactory, which is all the more remarkable that, while experiments and mean field are concerned with frictional balls, the simulations relate to the frictionless case. This is to be related with our previous observation that in the hcp lattice studied here, the normal stiffness is only weakly sensitive to shear interball forces. Such might not be the case for other ball arrays.

As is well known, since mean-field theories are not systematic expansions in powers of a small parameter, they do not allow for a precise direct assessment of their range of validity. From this discussion, we can state empirically that the validity of our effective medium approximation is limited to dimensionless forces $f^* \gtrsim 0.08$. This we confirm by calculating, within the mean-field approximation itself, the relative force fluctuations $\Delta f^*/f^* = \Delta \tilde{f}/\tilde{f}$, and $\Delta F_{\mathrm{av}}/F_{\mathrm{av}}$, where

$$(\Delta f)^2 = \sum_Q c_Q [F^Q(a) - K^Q u^Q - \tilde{f}(a)]^2. \qquad (50)$$

The plot of Fig. 9 shows that the relative fluctuations decrease rapidly with increasing displacement, i.e., pressure, the above mentioned empirical limit corresponding to the reasonable value $\Delta f^*/f^* \simeq 0.6$. The reduction of the local stress (force) fluctuations due to the self-consistent local displacements is reflected in the relative magnitude of the EMA and AFA fluctuations. The frictionless balls appear to adjust their positions more effectively, as could be expected.

Finally, we have estimated the average fraction of active contacts per ball N_c in our effective lattice in the following way. We define it to be the average number of neighbors with an intercenter distance smaller than the sum of the corresponding radii.

$$N_c = \sum_{Q,Q'} c_Q c_{Q'} \vartheta\left(\frac{d_Q + d_{Q'}}{2} - a - u_Q\right). \qquad (51)$$

Note that this expression does not derive systematically from the mean-field formalism, in which the notion of contact number does not enter explicitly. It should therefore be considered as indicative only. N_c is plotted on Fig. 10 together with the values calculated by Roux. Expression (51) is seen to systematically underestimate N_c. It appears that the valid-

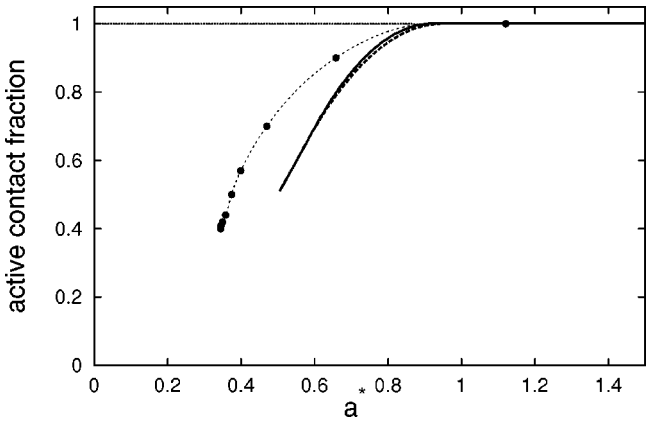

FIG. 10. Active contact fraction vs dimensionless displacement. Full line: EMA for frictional balls. Thick dashed line: EMA for frictionless balls. Dots: numerical simulation [7].

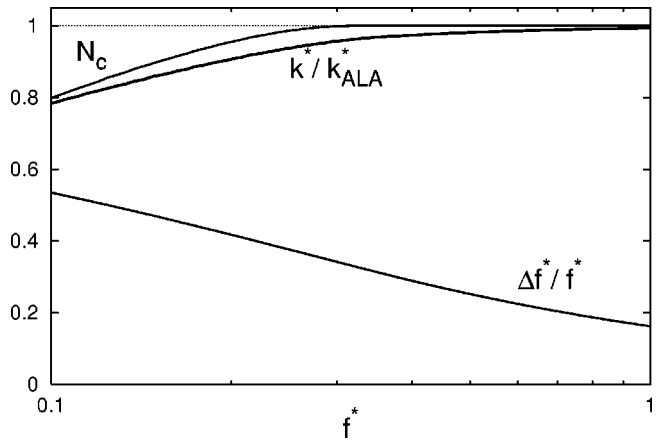

FIG. 11. The relative departure k^*/k^*_{ALA} of the EMA effective normal stiffness from ideal Hertz and the EMA force fluctuation $\Delta f^*/f^*$ exhibit no sharp change at the point $f^* \simeq 0.3$, where the active contact fraction N_c saturates to 1.

ity of the mean field extends down to $N_c \sim 85\%$. However, it is important to point out that the pressure range where the sound velocity departs from the Hertz behavior extends well into the pressure range where the contact fraction has already saturated to 1. This corroborates strongly the idea that it is not the connectivity itself which is responsible for the non-Hertz behavior, but the presence of disorder induced stress fluctuations. This is shown in Fig. 11, where we plot together the EMA results for $N_c, \Delta f^*/f^*$ and the ratio $\tilde{k}/k_{\mathrm{ALA}}$. This latter quantity is a direct measure of the deviations of the effective stiffness from the ideal Hertz law. No sharp change of regime occurs at saturation of N_c, the non-Hertz behavior and stress fluctuations appear to extend to higher pressures and gradually tend to zero together.

V. CONCLUSION

On the basis of the above discussion, we are therefore able to conclude that our mean-field theory provides quite a satisfactory description of the pressure dependence of the bulk mechanical properties, and hence of the sound velocity, in an array of frictional balls in the high-pressure range. This corresponds to the regime in which the ball network is strongly overdetermined, that is, where connectivity is close to its saturation value.

We believe that this agreement, which permits to account for the non-Hertz behavior down to the $\nu \approx \frac{1}{4}$ range, is due to the fact that this theory does capture, though in an approximate manner, the existence of disorder induced stress fluctuations, and that these are self-consistently related with the global mechanical state of the system. In other words, the true disorder strength in the problem is not intrinsically given by the dispersion of unstressed ball diameters, but determined from this *together with* the elastic deformation field.

We have based our single-site description upon the simplest possible approximation, which amounts to a spherical averaging of local lattice distortions. That this is sufficient to produce a satisfactory theory must certainly be attributed to the high connectivity of the hcp structure. It should for this reason be applicable as well to a 3D lattice such as the fcc one. This would be an additional check of the EMA because of the different topology of the 3D lattice, and it would at last provide a theoretical counterpart to the pioneering experiments of Ref. [2].

Systematic improvement upon this approximation is possible. This should be based on extending the basic building block from our (central ball) + (average bond star) to a full cluster made of the central ball and of its six neighbors. Such an extension, although obviously heavy, would have the merit of explicitly allowing for local asymmetric configurations, which we have ignored here. It would replace the conjecture (41) by a direct treatment of the shear interactions between the balls, permitting hence to study macroscopic shears in the same manner. It would also be a first step towards taking into account spatial stress correlations, which are completely overlooked in the present approach.

In view of this last remark, the good agreement obtained here with sound velocity data calls for a physical comment. Coherent sound measures a mechanical response on the scale of the corresponding effective wavelength which, in the low frequency regime of the Gilles-Coste experiments, is at least of the order of ten ball diameters, as discussed in Sec. IV. It is now well documented [7,8,22] that the correlation length of the stress network in granular packings is, at most, of the order of a few d. It is therefore to be expected that mean-field theories, though by nature unable to capture long range correlations, are well adapted to describe large scale properties. That is, when focusing on large scale mechanical responses, the pertinent notion is that of a global fluctuating stress network. The complementary notion of stress chains, which emphasizes the long range part of correlations, is certainly more relevant to the question of acoustic scattering which becomes essential at higher frequencies.

Obviously, an important pending question is concerned with the possibility of extending the mean-field approach to the more important case of topologically disordered random grain packings. Such a step, however desirable it might be, is by no means straightforward, as can be inferred from the, yet insuperable, difficulties that have been met when trying to extend the theories of electronic and vibrational properties of random substitutional alloys to amorphous materials. These can be assigned to the absence of a natural reference configuration possessing long range order. Up to now, the only existing theoretical frame for amorphous solids is a structureless, homogeneous effective medium. This would amount in the present problem to treating the effective medium in the continuum limit, which is clearly inadequate to account for stress fluctuation effects. In this perspective, numerical studies appear essential as a basis for trying to build up the needed original theoretical concepts.

However, we believe that the qualitative idea that emerges from this work, namely, that it is the disorder induced stress fluctuations that are responsible for the pressure dependence of the sound velocity in granular packings, will carry over, as well, to topologically disordered systems.

ACKNOWLEDGMENTS

We are grateful to C. Coste, B. Gilles, and J. N. Roux for fruitful discussions and for communication of their results

prior to publication. B.V. gratefully acknowledges the hospitality of Université Paris VII. This work was also supported in part by the grant agency of the Charles University of Prague (Project No. 146/1999).

APPENDIX: CALCULATION OF α, β

We want to calculate here the expression of the coefficients α, β defined in Sec. III. For this purpose, we need to solve the following problem. Consider an ideal hcp lattice, with interball distance at equilibrium d, in which we single out a central site (0). Apply to the six balls $i=1,...,6$ of the corona of its nearest neighbors excess forces directed along the $(0i)$ bonds $\mathbf{F}_i=F\hat{\mathbf{n}}_i$ (see Fig. 4). Call $\mathbf{u}_i=u_i\hat{\mathbf{n}}_i$ the resulting displacement of nearest neighbor i. Then, by definition, $\alpha=u_{i\alpha}/u_i$, where $\mathbf{u}_{i\alpha}$ is the displacement of the second neighbor $(i\alpha)$ along the $\hat{\mathbf{n}}_i$ direction; $\beta=u_{i\beta}/u_i$, with $\mathbf{u}_{i\beta}$ being the displacement of the next nearest neighbor along the direction of $(1/\sqrt{3})\hat{\mathbf{n}}_i+\hat{\mathbf{n}}_{i+1}$.

In order to avoid excessive algebraic heaviness, and in view of the fact that numerical studies lead us to conclude to the very weak sensitivity of the mean-field results to moderate variations of α, β, we limit ourselves to the simple case of vanishing Mindlin shear stiffness, $\eta=0$.

In this case rotations become irrelevant and, in the linear response regime, the force on a ball is related to the displacements of its neighbors by

$$\mathbf{F}_i=\sum_{\{j\}}\overline{\overline{D}}_{ij}\mathbf{u}_j \tag{A1}$$

so that, inverting in Fourier space,

$$\mathbf{u}_i=\sum_{\mathbf{k}}e^{i\mathbf{q}\cdot\mathbf{R}_i}\overline{\overline{\Delta}}(\mathbf{q})\mathbf{F}(\mathbf{q}) \tag{A2}$$

with

$$\overline{\overline{\Delta}}(\mathbf{q})=\overline{\overline{D}}^{-1}(\mathbf{q}). \tag{A3}$$

From Eq. (9), $\overline{\overline{D}}(\mathbf{q})$ is a 2×2 matrix acting in (x,y) space, defined by

$$\overline{\overline{D}}(\mathbf{q})=\sum_{i,\{j\}}e^{i\mathbf{q}\cdot(\mathbf{R}_i-\mathbf{R}_j)}\overline{\overline{D}}_{ij}=2k\sum_{p=1}^{3}[1-\cos(d\mathbf{q}\cdot\hat{\mathbf{n}}_p)]\hat{\mathbf{n}}_p\hat{\mathbf{n}}_p. \tag{A4}$$

The applied forces are defined by

$$\mathbf{F}_i=F[\hat{\mathbf{n}}_1(\delta_{i1}-\delta_{i4})+\hat{\mathbf{n}}_2(\delta_{i3}-\delta_{i6})+\hat{\mathbf{n}}_3(\delta_{i5}-\delta_{i2})], \tag{A5}$$

where the unit vectors $\hat{\mathbf{n}}_p$ and the sites i are labeled according to Fig. 1.

Then

$$\mathbf{F}(\mathbf{q})=\frac{f}{N}\sum_{p=1}^{3}(-2i)\hat{\mathbf{n}}_p\sin(d\mathbf{q}\cdot\hat{\mathbf{n}}_p), \tag{A6}$$

N being the number of sites in the lattice.

Taking advantage of the fact that, by symmetry, $\hat{\mathbf{n}}_1\cdot(\mathbf{u}_1-\mathbf{u}_4)=\hat{\mathbf{n}}_2\cdot(\mathbf{u}_3-\mathbf{u}_6)=\hat{\mathbf{n}}_3\cdot(\mathbf{u}_5-\mathbf{u}_2)$, one gets

$$u_1=\frac{\hat{\mathbf{n}}_1\cdot(\mathbf{u}_1-\mathbf{u}_4)}{2}=\frac{f}{3N}\sum_{\mathbf{q}}\sum_{p,r=1}^{3}\hat{\mathbf{n}}_p\overline{\overline{\Delta}}(\mathbf{q})\cdot\hat{\mathbf{n}}_r \times\{\cos[d\mathbf{q}\cdot(\hat{\mathbf{n}}_p-\hat{\mathbf{n}}_r)]-\cos[d\mathbf{q}\cdot(\hat{\mathbf{n}}_p+\hat{\mathbf{n}}_r)]\}. \tag{A7}$$

Analogously, the displacement $u_{1\alpha}$ of the second neighbor along Ox,

$$u_{1\alpha}=\frac{f}{3N}\sum_{\mathbf{q}}\sum_{p,r=1}^{3}\hat{\mathbf{n}}_p\cdot\overline{\overline{\Delta}}(\mathbf{q})\cdot\hat{\mathbf{n}}_r\{\cos[d\mathbf{q}\cdot(2\hat{\mathbf{n}}_p-\hat{\mathbf{n}}_r)] -\cos[d\mathbf{q}\cdot(2\hat{\mathbf{n}}_p+\hat{\mathbf{n}}_r)]\}. \tag{A8}$$

From Eqs. (3) and (4)

$$\mathcal{D}(\mathbf{q})=\det[\overline{\overline{D}}(\mathbf{q})]=\sum_{p=1}^{3}\Gamma_p\Gamma_{p+1} \tag{A9}$$

with

$$\Gamma_p=1-\cos(d\mathbf{q}\cdot\hat{\mathbf{n}}_p),\quad \Gamma_{p+3}\equiv\Gamma_p. \tag{A10}$$

Finally, one obtains, for $\alpha=u_{1\alpha}/u_1$,

$$\alpha=\frac{\sum_{\mathbf{q}}\mathcal{D}^{-1}(\mathbf{q})\sum_{p=1}^{3}\Gamma_p(\Sigma_{p+1}^{(2)}-\Sigma_{p+2}^{(2)})(\Sigma_{p+1}^{(1)}-\Sigma_{p+2}^{(1)})}{\sum_{\mathbf{q}}\mathcal{D}^{-1}(\mathbf{q})\sum_{p=1}^{3}\Gamma_p(\Sigma_{p+1}^{(1)}-\Sigma_{p+2}^{(1)})^2}, \tag{A11}$$

where we have set

$$\Sigma_p^{(n)}=\sin(nd\mathbf{q}\cdot\hat{\mathbf{n}}_p),\quad T_p=\sin(d\mathbf{q}\cdot\hat{\mathbf{t}}_p). \tag{A12}$$

A completely analogous calculation involving the displacement $u_{1\beta}$ of the second nearest neighbor yields

$$\beta=\frac{\sum_{\mathbf{q}}\frac{2}{\sqrt{3}}\mathcal{D}^{-1}(\mathbf{q})\sum_{p=1}^{3}\Gamma_p\left(T_p-\frac{T_{p+1}+T_{p+2}}{2}\right)(\Sigma_{p+1}^{(1)}-\Sigma_{p+i}^{(2)})}{\sum_{\mathbf{q}}\mathcal{D}^{-1}(\mathbf{q})\sum_{p=1}^{3}\Gamma_p\Sigma_{p+1}^{(1)}-\Sigma_{p+2}^{(1)})^2}. \tag{A13}$$

Performing numerically the $\mathbf{q}$ integrations over the Brillouin zone we obtain

$$\alpha=0.585\,405,\quad \beta=0.232\,971. \tag{A14}$$

[1] K. L. Johnson, *Contact Mechanics* (Cambridge University Press, Cambridge, 1985).
[2] J. Duffy and R. D. Mindlin, J. Appl. Mech. **24**, 585 (1957).
[3] B. Gilles and C. Coste, in *Powders and Grains 2001*, edited by Y. Kishino (Balkema, Lisse, 2001), p. 113.
[4] J. D. Goddard, Proc. R. Soc. London, Ser. A **430**, 105 (1990).
[5] P.-G. de Gennes, Europhys. Lett. **35**, 145 (1996).
[6] H. A. Makse, N. Gland, D. L. Johnson, and L. M. Schwartz, Phys. Rev. Lett. **83**, 5070 (1999).
[7] J. N. Roux, in *Powders and Grains 97*, edited by R. Behringer and J. Jenkins (Balkema, Rotterdam, 1997), p. 215; *Physique et Mecanique des Milieux Granulaires* (LCPC, Champs sur Marne, 2000).
[8] P. J. Digby, J. Appl. Mech. **48**, 803 (1981).
[9] K. Walton, J. Mech. Phys. Solids **35**, 213 (1987).
[10] K. W. Winkler, Geophys. Res. Lett. **10**, 1073 (1983).
[11] P. Sheng, *Introduction to Wave Scattering, Localization and Mesoscopic Phenomena* (Academic, San Diego, 1995).
[12] S. Feng, M. F. Thorpe, and E. Garboczi, Phys. Rev. B **31**, 276 (1985).
[13] L. M. Schwartz, S. Feng, M. F. Thorpe, and P. N. Sen, Phys. Rev. B **32**, 4607 (1985).
[14] S. Kirkpatrick, Rev. Mod. Phys. **45**, 574 (1973).
[15] L. M. Schwartz, D. L. Johnson, and S. Feng, Phys. Rev. Lett. **52**, 831 (1984).
[16] Note that at applied forces where this condition would not hold, the normal stress within the contact would reach a level comparable with the yield stress of the material, and plastic effects would have to be taken into account.
[17] X. Jia, C. Caroli, and B. Velický, Phys. Rev. Lett. **82**, 1863 (1999).
[18] F. Radjai, M. Jean, J. J. Moreau, and S. Roux, Phys. Rev. Lett. **77**, 274 (1996).
[19] We use the shorthand x_+^α for a function which is zero for $x<0$ and equals x^α for $x\geqslant 0$.
[20] Approximations closely resembling the ones described here are known in various areas. Thus, the averaged lattice approximation corresponds to the virtual crystal approximation in alloy physics and to the Reuss approximation in mechanics, while the averaged force approximation lies between the atomic limit approximation and the averaged *t*-matrix approximation in solid state physics, and is known as the Voigt approximation in mechanics.
[21] The well known D-EMT or differential effective medium theory also uses differential equations in the process of determining the effective elastic moduli of composites, but the control parameter is not the stress, but the fractional occupation of the sample by inclusions. The differential equation is obtained by a self-consistent extrapolation of the single inclusion limit. The theory dates back to the article: R. McLaughlin, Int. J. Eng. Sci. **15**, 237 (1977). A very recent work dealing with random inclusions and testing D-EMT against numerical simulations is: E. J. Garboczi and J. G. Berryman, Mech. Mater. **33**, 455 (2001).
[22] B. Miller, C. O'Hern, and R. P. Behringer, Phys. Rev. Lett. **77**, 3110 (1996).